Sensor applications

Adipose Tissue Characterization With Electrical Impedance Spectroscopy and Machine Learning

Florian Dapsance[1,2,3]* , Jie Hou[1,4]* , Damien Dufour[2,3] , Charlotte Boccara[2,3] ,
Nolwenn Briand[2] , and Ørjan Grøttem Martinsen[1,4]**

[1]Department of Physics, University of Oslo, NO-0316 Oslo, Norway
[2]Department of Molecular Medicine, Institute of Basic Medical Sciences, University of Oslo, NO-0316 Oslo, Norway
[3]Centre for Molecular Medicine Norway, University of Oslo, NO-0316 Oslo, Norway
[4]Department of Clinical and Biomedical Engineering, Oslo University Hospital, N-0424 Oslo, Norway
*Member, IEEE
**Senior Member, IEEE

Abstract—Biological tissues have variable passive electrical properties depending on their cellular constitution. Electrical impedance spectroscopy (EIS) is commonly used to monitor cell and tissue characteristics. By measuring the impedance of a sample at various frequencies, it is possible to collect information regarding cell size and shape, cell membrane properties, or cytoplasm conductivity. From the perspective of longitudinal structural monitoring, bioimpedance measurements outrank traditional tissue analysis methods, such as fixation and slicing, owing to their nondestructive nature. Machine learning can be used to automatically process the impedance data and make real-time classifications of tissue types. Here, we present preliminary results on ex-vivo mouse adipose tissue measurements using EIS and further data processing and classification using machine learning models.

Index Terms—Sensor applications, adipose tissue, bioimpedance, electrical impedance spectroscopy (EIS), machine learning.

I. INTRODUCTION

Electrical impedance spectroscopy (EIS) reveals the electric and dielectric properties of a material by measuring its response to an electric field over a range of frequencies. Bioimpedance, or bioelectrical impedance spectroscopy (BIS), focusing on biological samples, has raised significant interests for research and clinical applications [1], from biosensing of DNA [2], proteins [3], virus [4] or bacteria [5], to monitoring of mammalian cells [6], [7] and tissue [8], [9], [10]. In fact, the measured impedance data hold important information on the tissue structure, such as cell volume and cell-membrane properties [11], [12].

Adipose tissue is composed of adipocytes, which are cells that store a significant amount of fat within lipid droplets occupying most of the cell volume. White adipocytes contain a single lipid droplet and provide storage of energy in the form of triglycerides. Conversely, brown adipocytes contain multiple small lipid droplets and have the ability to dissipate energy in the form of heat instead of storing it.

In mice, white adipocytes can be found in visceral perigenital fat pads (gWAT) and subcutaneous inguinal depots (iWAT). Brown adipose tissue (BAT) is mainly found in the subcutaneous interscapular depot. Interestingly, and iWAT contains "beige" adipocytes harboring the features of brown adipocytes and interspersed within white adipose tissue [13].

Several studies have previously used EIS and machine learning approaches to classify different tissue types in vitro, for instance, breast tissue [14], lung tissue [15], and prostate cancer tissue [16]. To the best of authors' knowledge, no studies have focused on the use of EIS and machine learning to characterize and classify adipose tissues.

The most used method to analyze adipose tissue is tissue harvest, fixation, and slicing in 5–10 μm sections. This method, however, restricts usage for molecular analysis involving RNA or protein extraction, only providing a 2-D analysis. In contrast, EIS is nondestructive and could potentially be adapted for longitudinal monitoring of tissues in vivo.

In this letter, we designed an ex-vivo bioimpedance platform to map how the electric properties of adipose tissue may change between depots. To automatically classify adipose tissues, we tested several machine learning methods, using a support vector machine (SVM) and random forest (RF).

II. METHODS

A. Mice

The experimental use of animals was approved and registered by the Norwegian Animal Research Authority (Mattilsynet, KPM-IMB breeding protocol A057). Mice of both sexes were bred in-house and maintained on a C57Bl/6J genetic background. They were housed in individually ventilated plexiglass cages on a 12-h light/12-h dark cycle (lights on at 7:00 a.m.). They were fed normal, commercial rodent chow and provided with water ad libitum. Mice were terminated by cervical dislocation between 9 and 11 a.m. Adipose tissues were dissected and placed in phosphate-buffered saline (PBS) before measurement.

B. Bioimpedance Platform

To perform bioimpedance measurements on mouse adipose tissue, we designed a 3-D-printed polyethylene terephthalate glycol platform, including 7-mm-wide Ag/AgCl strip electrodes. The latter were electrically connected to 4-mm banana connectors and covered with epoxy glue at the soldered joint.
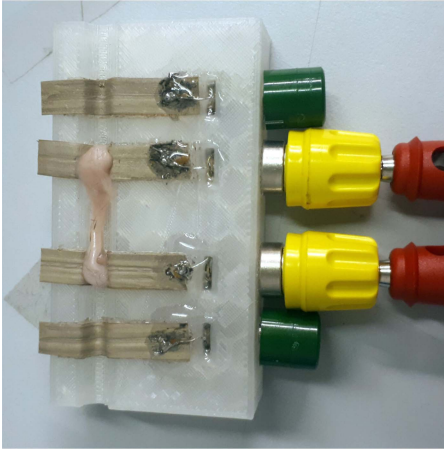
Fig. 1. Measurement of a mouse inguinal white adipose tissue sample on a custom-designed bioimpedance platform.

C. Measurement Protocol

The tissue was gently pressed against a piece of gauze to remove excess liquid from its surface and positioned on the platform between two electrodes (see Fig. 1). Signal generation and acquisition were operated by the commercially available Zurich Instruments MFIA 5 MHz Impedance Analyzer. This device was connected to the bioimpedance platform via shielded cables that were taped to the experiment bench. On the Zurich Instruments LabOne software, the excitation signal was initialized with a 100-mV peak voltage for a two-electrode setup over a 10–1 MHz frequency range. The surface of the electrode was softly cleaned with a piece of gauze between measurements and with 70% ethanol before and after each measurement session.

D. Machine Learning

Impedance data (both resistance and reactance) were used to train the models. For all the machine learning methods tested in this work, 80% of the total dataset was used as the training set (39 measurements), and 20% of the total dataset was used as the testing set (10 measurements). All data were normalized to unit norm using L2 normalization before entering the model. A grid search was performed for all the models so that the optimal hyperparameters were identified, resulting in the best model configuration.

E. Code Availability

Data visualization and principal component analysis (PCA) were carried out using Python 3, and Seaborn package was used for plots. All codes are available upon request without restriction.

III. RESULTS

A. Adipose Tissue Depots Have Different Bioimpedance Spectra

The following results were obtained by measuring adipose tissue depots from eight different mice. Two iWAT, two gWAT, and one BAT samples were collected per animal, resulting in 16 iWAT, 16 gWAT, and six BAT (two were discarded due to failed harvest) samples. Two iWAT, two gWAT, and one BAT samples were measured twice, changing the orientation lengthwise. One iWAT, one gWAT, and one BAT sample were measured three times in a row with a three-minute
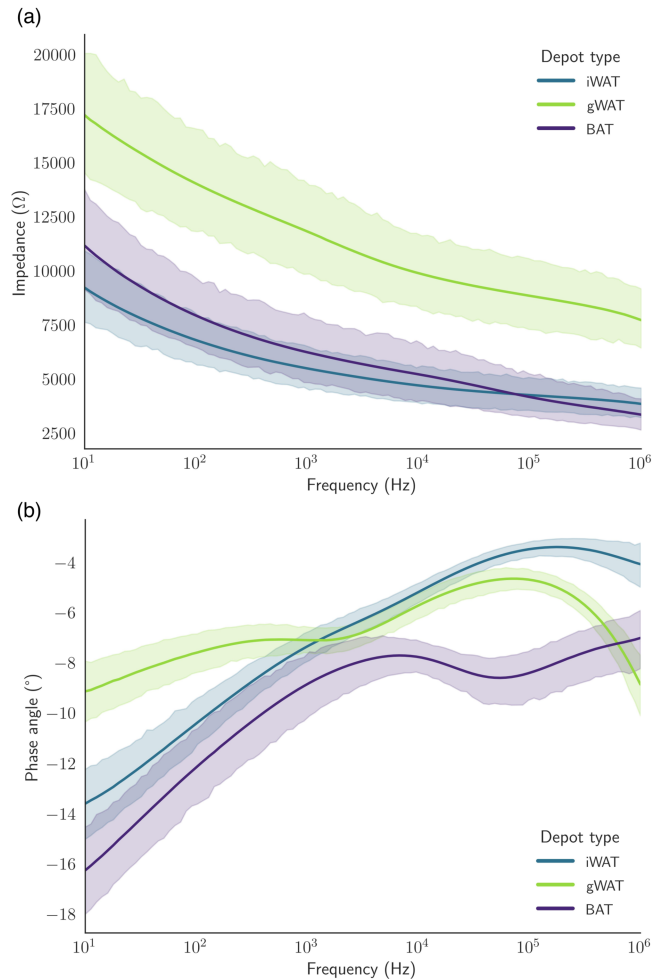

Fig. 2. (a) Average impedance and (b) phase angle spectra for each adipose tissue depot, iWAT, n = 20, gWAT, n = 20, and BAT, n = 9, with 95% confidence interval bands.

waiting interval. In total, we analyzed 20 iWAT, 20 gWAT, and 9 BAT bioimpedance measurement sets.

Fig. 2 shows the average impedance and phase angle for each adipose tissue depot type over the frequency range. The gWAT impedance decreases from 17 500 Ω at 10 Hz to 10 000 Ω at 10^4 Hz and 8000 Ω at 10^6 Hz. In contrast, both iWAT and BAT impedance responses are lower, with a common behavior between 10 and 10^4 Hz, decreasing from 9000–5000 Ω and from 11 500–5500 Ω, respectively. At higher frequencies, the iWAT and BAT impedances slightly diverge as they reach 4000 and 3500 Ω at 10^6 Hz, respectively. Impedance dynamics are expressed by the phase angle. The iWAT and BAT phase angles follow the same trend between 10 and 10^4 Hz and start differing from 2×10^3 Hz. Interestingly, the gWAT phase angle evolves differently between the lowest frequencies, from 10 to 2×10^3 Hz, and the highest frequencies, from 3×10^3 to 10^6 Hz, but very similarly to iWAT between 2×10^3 and 3×10^3 Hz.

To test our platform, we ran extra measurements with the same experimental setup. There was no significant variation in impedance nor in phase angle responses when flipping the sample lengthwise or when running multiple measurements on the same sample, placing it back in PBS between each data acquisition.

To determine whether our measurements were sensitive to our harvesting protocol, we evaluated the "air drying" effect with a short

Table 1. Average increase in impedance and absolute phase angle over the whole frequency range (10–10^6 Hz) over time compared with an initial measurement on iWAT ($n = 2$)

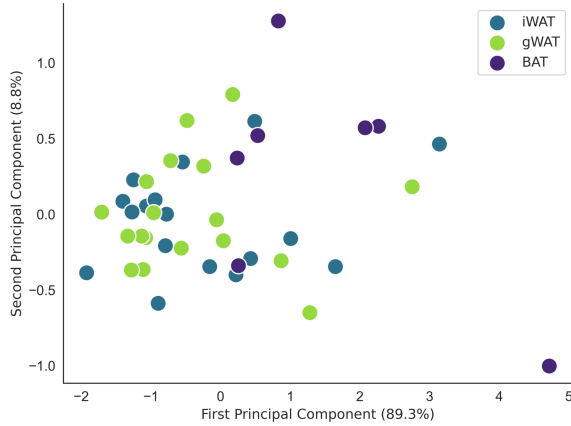| Drying time	Impedance	Phase angle
3 min	6.8%	6%
6 min	10.7%	7%
9 min	13.6%	7.7%

Fig. 3. Principal component analysis of iWAT, gWAT, and BAT impedance.

Table 2. Model parameters tested and best parameter values found together with accuracy achieved with SVM and RF models

Model	Model parameters	Best parameters	Accuracy
SVM	$C \in$ logspace(-5, 5, 11)	100	100%
RF	$N \in$ [500 - 1000]	800	90%

analysis. Indeed, each sample resting in PBS for a variable duration before a measurement may be coated with a variable amount of solution that impacts the tissue response. To test this effect, we performed several measurements in a row on the same iWAT sample with drying time periods of 3, 6, and 9 min. As expected, when compared with an initial acquisition, the impedance and absolute phase angle progressively increased over time as given in Table 1. We found an equivalent evolution with gWAT samples.

B. Machine Learning to Discriminate Adipose Tissue Depots

In order to automatically classify adipose tissue types, we ran a PCA on impedance data. The two first components were responsible for 89.3% and 88%, respectively, of the variation. PCA was not sensitive enough to discriminate between different tissues (see Fig. 3). To find a better way to predict the nature of the tissues based on their impedance, we used machine learning models. For the SVM, the regularization parameter "C" value range tested was between logspace(-5, 5, 11), and the best value found was 100. For the RM model, we tested between 500 and 1000 trees, with a step of 100, and found the best value to be 800. The models were run with the optimal parameters, with SVM, an accuracy of 100% was achieved, and with RF, an accuracy of 90% was achieved, as given in Table 2.

IV. DISCUSSION

We designed an ex-vivo bioimpedance platform to measure the passive electrical properties of mouse adipose tissues. From the impedance spectrum, we can clearly discriminate gWAT from iWAT and BAT. This is most likely explained by the cellular composition of each tissue. iWAT adipocytes are smaller in mice than gWAT adipocytes [17], and iWAT can also contain beige adipocytes, unlike gWAT, which makes it structurally closer to BAT than gWAT.

At low frequencies, below 10^4 Hz, electrical current mainly passes around cells because of the dominating capacitance of the cell membrane. Therefore, the extracellular architecture dominates a tissue's impedance. As the frequency increases, the cell membrane properties and the intracellular composition start to contribute to the impedance of tissue. At high frequencies, from 10^6–10^7 Hz, current flows everywhere according to local ionic conductivity.

As depicted in Fig. 2, the higher impedance response of gWAT implies that this tissue has larger cells, whereas iWAT and BAT seem to be more densely populated in cells. One major difficulty that arises when interpreting such results is that, although fat tissue is rich in low-conductivity materials (lipids), its electrical conductivity is particularly dependent on liquid distribution (e.g., vascularization, and intra- and extracellular spaces).

Furthermore, the phase angle gives an additional perspective on bioimpedance measurements. By definition, a high absolute phase angle is associated with a high reactance, or capacitance, compared with the resistance and, therefore, suggests a large influence from cell membranes. For our analyses, this meant that the phase angle we measured in each tissue could reflect the distribution of water between the extra- and intracellular spaces.

Our preliminary data suggest that the low-frequency range underlines the similarities between iWAT and BAT, while the 3×10^3–10^5 Hz range is where iWAT and gWAT are alike. These observations may provide evidence connecting the structural characteristics of adipose tissues with their passive electrical properties at specific frequency ranges.

Bioimpedance measurements with two electrodes are subject to electrode polarization, primarily at low frequencies. Hence, the obtained impedance results from the electrode/tissue interface in addition to the impedance of the tissue. We evaluated the impact of electrode polarization by comparing measurements at various electrode distances on our platform. Assuming a linear dependence between the measured impedance and the electrode distance, we assessed the polarization impedance to correspond to 50% of the measured impedance at 10 Hz. The polarization impedance to tissue impedance ratio decreases progressively down to 27% at 10^6 Hz. We believe this extrapolation to be overestimated due to the nonuniformity of the tissue and electrode/tissue interface causing a nonlinear polarization behavior. Furthermore, even at low frequencies, our measurements reveal a low phase angle, which indicates that the impedance is not dominated by high-capacitive effects. Despite the polarization effect, our data, including the lower part of the spectrum, prove to be still insightful in discriminating between adipose tissues.

We also plan to investigate adipose tissue response at high frequencies, 1–200 MHz and above, which may highlight new tissue properties.

We chose the SVM and RF models given the relatively small dataset. The phase angle data were also tested, and the same accuracies were achieved. The present work aims at demonstrating a proof of concept that EIS together with machine learning has the potential to classify different adipose tissues. With more data in the future, we plan to build deep learning models, using explainable artificial

intelligence methods to determine the most relevant frequencies that can discriminate between adipose tissues. This would enable us to achieve simplified instrumentation targeting only a few frequencies to distinguish different adipose tissue types.

V. CONCLUSION

Here, we demonstrated that combining the impedance and phase angle responses of mouse adipose tissue seems to be effective to distinguish between various depot types. iWAT, gWAT, and BAT exhibit specific behaviors, with divergences and similarities, over a wide range of frequencies. These results are preliminary and should be further confirmed to be considered.

Bioimpedance measurements provide a rapid, real-time, cheap, and nondestructive method for analyzing adipose tissue that could be adapted for in vivo longitudinal monitoring. It is a promising alternative to histological methods requiring the use of fixative chemicals. We further propose that machine learning models can be used to perform real-time classification of the tissue type from one single raw data acquisition. Such strategies will complement more traditional approaches that interpret bioimpedance experiments by building an equivalent circuit model while attempting to fit measured data.

ACKNOWLEDGMENT

REFERENCES

[1] S. Abasi, J. R. Aggas, G. G. Garayar-Leyva, B. K. Walther, and A. Guiseppi-Elie, "Bioelectrical impedance spectroscopy for monitoring mammalian cells and tissues under different frequency domains: A review," *Amer. Chem. Soc. Meas. Sci. Au*, vol. 2, no. 6, pp. 495–516, Dec. 2022, doi: 10.1021/acsmeasuresciau.2c00033.

[2] F. Heimbach et al., "Measurement of changes in impedance of DNA nanowires due to radiation induced structural damage," *Eur. Phys. J. D*, vol. 71, no. 8, Aug. 2017, Art. no. 211, doi: 10.1140/epjd/e2017-70819-1.

[3] D. Zhang et al., "Protein detecting with smartphone-controlled electrochemical impedance spectroscopy for point-of-care applications," *Sensors Actuators B: Chem.*, vol. 222, pp. 994–1002, Jan. 2016, doi: 10.1016/j.snb.2015.09.041.

[4] X. Li et al., "Enhancing the performance of paper-based electrochemical impedance spectroscopy nanobiosensors: An experimental approach," *Biosensors Bioelectron.*, vol. 177, Apr. 2021, Art. no. 112672, doi: 10.1016/j.bios.2020.112672.

[5] M. A. Nahid, C. E. Campbell, K. S. K. Fong, J. C. Barnhill, and M. A. Washington, "An evaluation of the impact of clinical bacterial isolates on epithelial cell monolayer integrity by the electric cell-substrate impedance sensing (ECIS) method," *J. Microbiological Methods*, vol. 169, Feb. 2020, Art. no. 105833, doi: 10.1016/j.mimet.2020.105833.

[6] C. Canali et al., "Bioimpedance monitoring of 3D cell culturing—Complementary electrode configurations for enhanced spatial sensitivity," *Biosensors Bioelectron.*, vol. 63, pp. 72–79, Jan. 2015, doi: 10.1016/j.bios.2014.07.020.

[7] L. L. Crowell, J. S. Yakisich, B. Aufderheide, and T. N. G. Adams, "Electrical impedance spectroscopy for monitoring chemoresistance of cancer cells," *Micromachines*, vol. 11, no. 9, Aug. 2020, Art. no. 832, doi: 10.3390/mi11090832.

[8] P. C. Calvo, O. Campo, C. Guerra, S. Castaño, and F. Fonthal, "Design of using chamber system based on electrical impedance spectroscopy (EIS) to measure epithelial tissue," *Sens. Biosensing Res.*, vol. 29, Aug. 2020, Art. no. 100357, doi: 10.1016/j.sbsr.2020.100357.

[9] G. Company-Se et al., "Minimally invasive lung tissue differentiation using electrical impedance spectroscopy: A comparison of the 3- and 4-electrode methods," *IEEE Access*, vol. 10, pp. 7354–7367, 2022, doi: 10.1109/ACCESS.2021.3139223.

[10] S. L. Hillary, B. H. Brown, N. J. Brown, and S. P. Balasubramanian, "Use of electrical impedance spectroscopy for intraoperative tissue differentiation during thyroid and parathyroid surgery," *World J. Surg.*, vol. 44, no. 2, pp. 479–485, Feb. 2020, doi: 10.1007/s00268-019-05169-7.

[11] D. A. Dean, T. Ramanathan, D. Machado, and R. Sundararajan, "Electrical impedance spectroscopy study of biological tissues," *J. Electrostatics*, vol. 66, no. 3, pp. 165–177, Mar. 2008, doi: 10.1016/j.elstat.2007.11.005.

[12] D. D. Stupin et al., "Bioimpedance spectroscopy: Basics and applications," *Amer. Chem. Soc. Biomaterials Sci. Eng.*, vol. 7, no. 6, pp. 1962–1986, Jun. 2021, doi: 10.1021/acsbiomaterials.0c01570.

[13] A. Sakers, M. K. De Siqueira, P. Seale, and C. J. Villanueva, "Adipose-tissue plasticity in health and disease," *Cell*, vol. 185, no. 3, pp. 419–446, Feb. 2022, doi: 10.1016/j.cell.2021.12.016.

[14] C. Liu, T. Chang, and C. Li, "Breast tissue classification based on electrical impedance spectroscopy," in *Proc. Int. Conf. Ind. Technol. Manage. Sci.*, 2015, pp. 237–240, doi: 10.2991/itms-15.2015.56.

[15] R. Baghbani, M. B. Shadmehr, M. Ashoorirad, S. F. Molaeezadeh, and M. H. Moradi, "Bioimpedance spectroscopy measurement and classification of lung tissue to identify pulmonary nodules," *IEEE Trans. Instrum. Meas.*, vol. 70, pp. 1–7, Aug. 2021, doi: 10.1109/TIM.2021.3105241.

[16] M. A. Shini, S. Laufer, and B. Rubinsky, "SVM for prostate cancer using electrical impedance measurements," *Physiol. Meas.*, vol. 32, no. 9, pp. 1373–1387, Sep. 2011, doi: 10.1088/0967-3334/32/9/002.

[17] P. R. Johnson and J. Hirsch, "Cellularity of adipose depots in six strains of genetically obese mice," *J. Lipid Res.*, vol. 13, no. 1, pp. 2–11, Jan. 1972, doi: 10.1016/S0022-2275(20)39428-1.